

Radiance–irradiance inversion algorithm for estimating the absorption and backscattering coefficients of natural waters: vertically stratified water bodies

Howard R. Gordon and G. Chris Boynton

A full multiple-scattering algorithm for inverting profiles of the upwelling and downwelling irradiances to yield profiles of the absorption and backscattering coefficients in a vertically stratified water body is described and tested with simulated data. The algorithm does not require knowledge of the scattering phase function of the medium. The results are better the closer the phase function assumed in the retrievals is to the true phase function, although excellent retrievals of the absorption coefficient can still be obtained with an inaccurate phase function. Simulations show that the algorithm is capable of determining the vertical structure of a stratified water body and usually provides the absorption coefficient profile with an error $\leq 2\%$ and the backscattering coefficient profile with an error $\leq 10\%$, as long as the spacing between pseudodata samples is sufficiently small that the necessary derivatives of the irradiances can be accurately computed. The performance is only slightly degraded when the upwelling radiance (nadir viewing) is substituted for the upwelling irradiance. © 1998 Optical Society of America
OCIS codes: 010.0010, 010.4450, 290.0290, 290.1350, 290.4210.

1. Introduction

In an earlier paper we¹ reported an iterative algorithm for retrieving the absorption coefficient a and the backscattering coefficient b_b of a homogeneous water body from the measurement of depth profiles of the upward and downward irradiances E_u and E_d or the nadir-viewing radiance L_u , and E_d . The algorithm accounted for all significant orders of multiple scattering. An attractive feature was that it did not require precise knowledge of the scattering phase function of the medium. For the E_u – E_d algorithm, the error in the retrieved a and b_b usually were found to be $\leq 1\%$ and 10–20%, respectively. The performance of the L_u – E_d algorithm was not as good, being more sensitive to the scattering phase function assumed in the inversions. The algorithm was extended to accommodate the presence of a Lambertian reflecting bottom, and tests showed that it was still possible to retrieve a ; however, in this case, the retrievals of b_b could contain large errors.

In this paper we extend the algorithm to a verti-

cally stratified water body. First we present the details of the algorithm. Next, using pseudodata, we present a series of tests in which the algorithm is applied to a homogeneous medium and a medium in which the optical properties are continuously stratified. Finally we consider situations in which the performance of the algorithm can be degraded, e.g., the presence of thin layers that cannot be resolved given the vertical density of the irradiance data.

2. Inversion Algorithm

We begin with a brief review of our E_u – E_d algorithm for a homogeneous water body and then provide the extension to a stratified water body.

A. Homogeneous Water Body

At any depth z in the medium, the absorption coefficient can be obtained from the irradiances by use of Gershun's law,² i.e.,

$$a(z) = \bar{\mu}(z)K_v(z), \quad (1)$$

where $\bar{\mu}(z)$ is the average cosine of the radiance distribution, $\bar{\mu}(z) \equiv [E_d(z) - E_u(z)]/E_0(z)$; $E_0(z)$ is the scalar irradiance; and $K_v(z) \equiv -d/dz\{\ln[E_d(z) - E_u(z)]\}$ is the attenuation coefficient of the vector or net irradiance. Equation (1) is exact, and in our algorithm it is used at each step in the iteration. Unfortunately there is no exact relationship for b_b

The authors are with the Department of Physics, University of Miami, Coral Gables, Florida 33124.

Received 3 November 1997; revised manuscript received 6 March 1998.

0003-6935/98/183886-11\$15.00/0

© 1998 Optical Society of America

similar to Eq. (1). In our algorithm, b_b is obtained from the irradiance reflectance, $R(z) \equiv E_u(z)/E_d(z)$, by use of a relationship for R that is approximately valid near the surface:^{3,4} $R \approx 0.33b_b/a$. We assumed that this relationship is valid (locally) at all depths, so

$$b_b(z) = 3R(z)a(z) \quad (2)$$

provides b_b from the measured value of R and the computed value of a at each depth. As the water body is assumed to be homogeneous, i.e., $a(z)$ and $b_b(z)$ are independent of z , the constant values for these properties are obtained by computing average values of these quantities (weighted by E_d or by $\ln E_d$) over depth.

Given $E_d(z)$ and $E_u(z)$, $a(z)$ and $b_b(z)$ could be obtained from Eqs. (1) and (2) if $\bar{\mu}(z)$ were known. In our algorithm, $\bar{\mu}(z)$ is determined iteratively by solving the radiative transfer equation (RTE) by use of trial values of a and b_b . The full procedure works in the following manner. First, to start the algorithm we need estimates of a and b_b . We achieved the a estimate by replacing $\bar{\mu}(z)$ in Eq. (1) by μ_0 , the cosine of the solar zenith angle in the water, i.e., by assuming that there is no atmosphere and no scattering in the water. This initial guess for $a(z)$ is then used to provide an initial guess for $b_b(z)$ with Eq. (2). Next, a scattering phase function $P(\Theta)$, where Θ is the scattering angle, is assumed for the medium, and the backscattering probability \widetilde{b}_b is computed from

$$\widetilde{b}_b = 2\pi \int_{\pi/2}^{\pi} P(\Theta) \sin \Theta d\Theta.$$

However, $\widetilde{b}_b = b_b/b$, where b is the total scattering coefficient of the medium. Thus, given $b_b(z)$ and the scattering phase function, we are able to determine the scattering coefficient. The inherent optical properties (IOP's) a , b , and $P(\Theta)$ are then introduced into the RTE, which is solved for the irradiances $E_d(z)$, $E_u(z)$, and $E_0(z)$. These irradiances provide a new estimate of the average cosine $\bar{\mu}(z)$ and a computed profile of $R(z)$. This estimate of $\bar{\mu}(z)$ is then used to obtain a new estimate of $a(z)$ by Eq. (1), and $a(z)$ and the difference between the computed and true profiles of $R(z)$ are then used to determine $b_b(z)$ by Eq. (2). This process is continued until the residual error after n iterations, defined as

$$\delta^{(n)} = \frac{1}{2N} \sum_{i=1}^N |\ln[E_d^{(n)}(z_i)] - \ln[E_d(z_i)]| + \frac{1}{2N} \times \sum_{i=1}^N |\ln[E_u^{(n)}(z_i)] - \ln[E_u(z_i)]|, \quad (3)$$

reaches a minimum. This results in values of a and b_b that, when inserted into the RTE (with the assumed phase function), reproduce the irradiance data.

B. Vertically Stratified Water Body

Equation (1) is exact and therefore can also be applied in a vertically stratified medium. In contrast, the approximation leading to Eq. (2) is valid only for homogeneous media, and then only for $z = 0$. This is because $R(z')$ is dependent on the optical properties of the water for $z > z'$. Thus an alternate approach is required to estimate $b_b(z)$.

Based on the research of Gordon and McCluney⁵ and Gordon,⁶ Gordon and Clark⁷ showed that the irradiance reflectance just beneath the surface ($z = 0^-$) of a vertically stratified water body is approximately given by

$$R(0^-) \approx \frac{\langle X(0^-) \rangle}{3},$$

where

$$\langle X(0^-) \rangle \equiv \frac{\int_0^{z_{90}} X(z)g(z)dz}{\int_0^{z_{90}} g(z)dz},$$

$$g(z) = [E_d(z)/E_d(0)]^2,$$

$$X(z) = b_b(z)/a(z).$$

The quantity z_{90} is called the penetration depth⁵ and is the depth above which 90% of the upwelling irradiance at the surface is scattered, and also the depth over which the downwelling irradiance falls to $1/e$ of its value at the surface. Following the spirit of the homogeneous medium algorithm, we assume that a similar equation is valid at all depths, i.e.,

$$R(z) \approx \frac{\langle X(z) \rangle}{3}, \quad (4)$$

where

$$\langle X(z) \rangle = \frac{\int_z^{z_{90}'} X(z')g(z, z')dz'}{\int_z^{z_{90}'} g(z, z')dz'}$$

$$g(z, z') = [E_d(z')/E_d(z)]^2,$$

where $z' \geq z$, and z_{90}' is the depth over which $E_d(z')$ falls to $1/e$ of its value at $z = z'$. As relationship (4) is only approximate, for simplicity we carry out the vertical integrations from the depth $z' = z$ down to the maximum depth at which irradiance data are obtained (z_{\max}). Approximation (4) can be solved for $X(z)$ given the $R(z)$ profile:

$$X(z) = 3 \left\{ R(z) - \frac{dR(z)}{dz} \int_z^{z_{\max}} dz' \left[\frac{E_d(z')}{E_d(z)} \right]^2 \right\}. \quad (5)$$

Because $a(z)$ can be estimated from Eq. (1), $X(z)$ provides $b_b(z)$. Note that replacement of z_{90}' by z_{\max} is

a good approximation only if $dR(z)/dz \rightarrow 0$ as $z \rightarrow z_{\max}$.

By use of these estimates the algorithm proceeds in a manner similar to the homogeneous medium case. Let the measured values of the downwelling irradiance and the upwelling irradiances be denoted by $E_d^m(z)$ and $E_u^m(z)$, respectively. These provide the measured reflectance $R^m(z)$ and the measured vector irradiance attenuation coefficient $K_v^m(z)$. The algorithm is initialized by approximating $\bar{\mu}(z)$ by μ_0 , i.e.,

$$a^0(z) = \mu_0 K_v^m(z), \quad b_b^0(z) = a^0(z) X^m(z),$$

where $X^m(z)$ is computed with $R^m(z)$ and $E_d^m(z)$ in Eq. (5). Then, making an assumption regarding the scattering phase function, which provides \widetilde{b}_b , the total scattering coefficient is found from

$$b^0(z) = \frac{b_b^0(z)}{\widetilde{b}_b(z)}.$$

The quantities $a^0(z)$, $b^0(z)$, and the assumed phase function are then introduced into the RTE that is solved for the irradiances $E_d^c(z)$, $E_u^c(z)$, and $E_0^c(z)$, providing a new estimate for $\bar{\mu}(z)$, which we call $\bar{\mu}^{(1)}(z)$. Then $\bar{\mu}^{(1)}(z)$ is used to provide a new estimate of the absorption coefficient profile, etc. Thus, going into the i th from the $(i - 1)$ th iteration, the absorption coefficient is approximated through

$$a^i(z) = \bar{\mu}^{(i-1)}(z) K_v^m(z),$$

i.e., the new absorption coefficient profile is always determined by the previous estimate of the average cosine.

Incrementation of the backscattering coefficient $b_b(z)$ from one iteration to the next is based on the difference between the current value of $X(z)$, i.e., $X^i(z)$, and the measured value $X^m(z)$. At the end of the i th iteration this difference is

$$\Delta X^i(z) = X^m(z) - X^i(z).$$

This would imply that $b_b(z)$ should be changed by

$$\Delta b_b^i(z) = \Delta X^i(z) a^i(z);$$

however, because Eq. (5) is not precise, we introduce a relaxation parameter⁸ f to stabilize the iteration procedure. The new estimate for the backscattering coefficient is then

$$b_b^i(z) = b_b^{i-1}(z) + f \Delta b_b^i(z),$$

where $0 < f < 1$. The fundamental difference between the present algorithm and that described in Subsection 2.A is the dR/dz term in Eq. (5).

As in the homogeneous case, the retrieved values of $a(z)$ and $b_b(z)$ are those for which δ^n in Eq. (3) is a minimum. The minimum is established by storing δ^n after each iteration and choosing the n value that provides a minimum. In reality, one never knows if an absolute minimum in δ^n is achieved. Thus we perform a number of tests to simply determine if a

relative minimum has been reached, or if significant progress is being made toward a minimum. Otherwise we stop the algorithm after 50 iterations.

In complete analogy with the homogeneous medium,¹ the algorithm utilizing $L_u(z)$ instead of $E_u(z)$ simply uses the value of $Q(z) \equiv E_u(z)/L_u(z)$ to derive $E_u(z)$ from the measured value of $L_u(z)$. $E_u(z)$ is then used in the algorithm as already described in this subsection. At each iteration, the profile $Q(z)$ is estimated. For the i th iteration the measured value of $E_u(z)$ is taken to be

$$E_u^m(z) = Q^{i-1}(z) L_u^m(z),$$

where $Q^{i-1}(z)$ is the estimate of $Q(z)$ after $i - 1$ iterations, and $L_u^m(z)$ is the actual measured quantity. Thus in the $L_u(z)$ - $E_d(z)$ algorithm the actual data used for the upwelling irradiances are changed along with $a(z)$ and $b_b(z)$ at each iteration.

The algorithm uses a Monte Carlo code as a subroutine to solve the RTE. This code includes a 50-layer atmosphere with both aerosol and Rayleigh scattering and has been thoroughly tested through comparison with other radiative transfer codes.⁹ Of course any of a number of well-known codes that are available, e.g., see Ref. 9, could be used as well.

3. Examples of the E_u - E_d Algorithm Performance

In this section we provide several representative examples that demonstrate the performance of the E_u - E_d algorithm.

A. Homogeneous Medium

Our first application of the algorithm was to test its ability to correctly determine the vertical structure of a homogeneous ocean. Figure 1 provides Monte Carlo simulations of the vertical profiles of $R(z)$ for a medium in which the $a(z) = 0.1 \text{ m}^{-1}$ and $b(z) = 0.9 \text{ m}^{-1}$ and for which the ocean is illuminated by the Sun at the zenith [Fig. 1(a)] and at a solar zenith angle θ_0 of 60° [Fig. 1(b)]. The scattering by the water body was governed by the Henyey-Greenstein¹⁰ (HG) phase function with an asymmetry parameter $g = 0.85$. There was no atmosphere above the ocean (Sun in a dark sky). The filled circles provide the true values of $R(z)$. Note the strong variation of $R(z)$ with depth, even though the IOP's are independent of depth. Clearly, Eq. (2) is a very poor approximation to the variation of $R(z)$ as a and b_b are both constant in this example. The pseudo-data generated in these simulations at the 20 depths shown in Fig. 1 were introduced into the E_u - E_d retrieval algorithm described in Subsection 2.B, and values of $a(z)$ and $b_b(z)$ were retrieved at each depth at which data were provided. The solid curve in Fig. 1 joins points of the computed value of $R(z)$ by use of the values $a(z)$ and $b_b(z)$ provided by the algorithm. These retrieved parameters reproduce the measured $E_d^c(z)$, $E_u^c(z)$, and $R(z)$ with an error of $\leq 0.5\%$. In this case the phase function used by the inversion algorithm was the correct one, i.e., a HG with $g = 0.85$. Figure 2 provides the error in the recovered

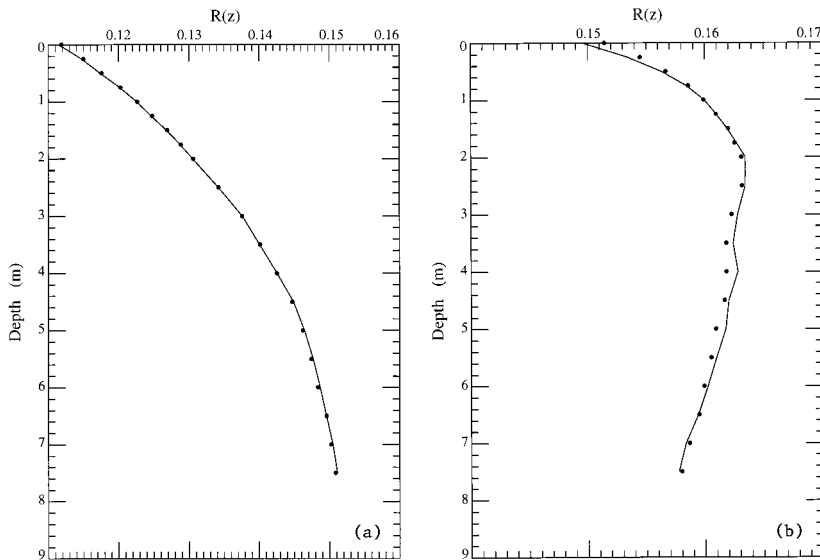


Fig. 1. $R(z)$ for a medium in which the $a(z) = 0.1 \text{ m}^{-1}$ and $b(z) = 0.9 \text{ m}^{-1}$. The filled circles are the values of $R(z)$ introduced into the algorithm as data (the pseudodata). The solid curve joins the points of the value of $R(z)$ computed with the values of $a(z)$ and $b_b(z)$ that were retrieved by the algorithm: (a) $\theta_0 = 0^\circ$, (b) $\theta_0 = 60^\circ$.

values of $a(z)$ [Fig. 2(a)] and $b_b(z)$ [Fig. 2(b)]. As with Fig. 1, the solid circles represent the true values, whereas the solid curves and broken curves represent the errors in the recovered values for $\theta_0 = 0$ and 60° , respectively. We note that the error in the recovered $a(z)$ is typically $<1\%$, whereas the error in $b_b(z)$ is usually $\leq 2\%$. Considering the strong variation of $R(z)$, Eq. (5) shows a remarkable ability to recognize the fact that the IOP's are independent of depth. Table 1 provides a summary of the errors for a variety of similar situations in which a and b_b are constant. The parameter ω_0 in the table is the single-scattering albedo, defined to be $b/(a + b)$. For Figs. 1 and 2, $\omega_0 = 0.9$. In Table 1, $\langle \Delta a \rangle$ and $\langle \Delta b_b \rangle$ are the averages over depth of the absolute value of the relative errors in $a(z)$ and $b_b(z)$, respectively, e.g.,

$$\langle \Delta a \rangle \equiv \frac{1}{N} \sum_{i=1}^N \left| \frac{a^{\text{retrieved}}(z_i) - a^{\text{true}}(z_i)}{a^{\text{true}}(z_i)} \right|, \quad (6)$$

where $a^{\text{retrieved}}(z_i)$ and $a^{\text{true}}(z_i)$ are the retrieved and true values of the absorption coefficient at a depth z_i , respectively. The quantities $(\Delta a)_{\text{max}}$ and $(\Delta b_b)_{\text{max}}$ are the maximum values obtained for the error in $a(z)$ and $b_b(z)$. (Throughout this paper when errors carry signs, a positive sign means that the computed or retrieved quantity is greater than the true quantity.) These maxima typically occur at or near the surface (Fig. 2) where numerical computation of the required derivatives is less accurate. (We use a three-point algorithm to compute the derivatives.) Clearly, the algorithm performs as well for other values of ω_0 as it did for $\omega_0 = 0.9$ in Figs. 1 and 2.

Comparison of $\langle \Delta a \rangle$ and $\langle \Delta b_b \rangle$ in Table 1 with the errors δa and δb_b for similar simulations made by use of the homogeneous medium algorithm (Table 1 of Ref. 1) shows that in these cases the homogeneous medium algorithm leads to smaller errors; however, it has the advantage of already knowing the vertical

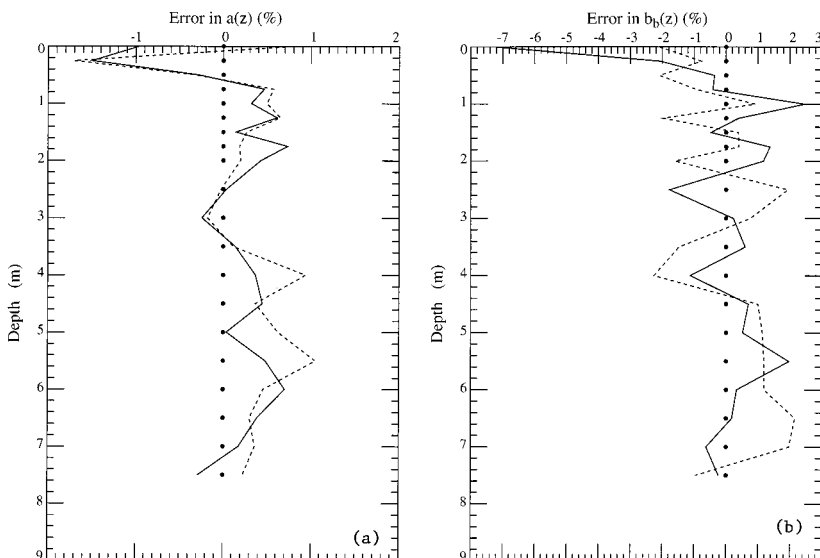


Fig. 2. Error in the recovered values of (a) $a(z)$ and (b) $b_b(z)$. The solid circles represent the true values, whereas the solid curves and broken curves join the errors in the recovered values for $\theta_0 = 0$ and 60° , respectively.

Table 1. Summary of the Average and Maximum Errors in Percent Obtained for $a(z)$ and $b_b(z)$ for a Homogeneous Medium^a

θ_0	ω_0	$\langle \Delta a \rangle$	$\langle \Delta b_b \rangle$	$(\Delta a)_{\max}$	$(\Delta b_b)_{\max}$
0°	0.2	1.36	2.26	-3.24	-4.98
60°	0.2	0.78	1.81	-2.68	+8.69
0°	0.4	0.87	1.01	+3.67	+2.54
60°	0.4	1.07	1.92	+4.91	+4.45
0°	0.6	0.88	0.85	-2.62	-2.81
60°	0.6	0.79	1.24	-3.00	+3.82
0°	0.8	0.67	0.79	+1.57	-2.34
60°	0.8	0.55	0.72	-1.15	-2.40
0°	0.9	0.44	1.21	-1.50	-7.24
60°	0.9	0.36	1.68	+1.55	-5.44
0°	0.95	0.53	3.60	+1.36	-17.54
60°	0.95	0.62	1.20	+3.86	-3.58

^aThe correct phase function was used in the retrieval.

structure of the water body—the present algorithm must determine the vertical structure.

B. Continuously Stratified Medium

To test the algorithm's performance when the medium is actually stratified, we devised profiles for $a(z)$ and $b_b(z)$ that had Gaussian shapes, i.e.,

$$a(z) = a_0 + a_1 \exp\left[-\frac{(z - z_a)^2}{2\sigma_a^2}\right],$$

$$b_b(z) = b_0 + b_1 \exp\left[-\frac{(z - z_b)^2}{2\sigma_b^2}\right],$$

where z_a and z_b are the depths of the maximal values of a and b_b , respectively, and the parameters a_1 , b_1 , σ_a , and σ_b control the magnitude of the maximal values above a_0 and b_0 and the depth range of the maxima. We simulated profiles for which either a_1 or b_1 was zero (no variation with depth) and for which $a_1 = a_0$ and/or $b_1 = b_0$. In addition, z_a and z_b were allowed to take on the values of 1, 2, or 3 m. In all cases, σ_a and σ_b were set to 1 m. Thus, over the range of depths from 0 to 5 m, $a(z)$ and $b_b(z)$ could each vary by as much as a factor of 2. The specific combinations of z_a , z_b , a_1 , and b_1 that we used in this test are provided in Table 2. In each case, $a_0 = 0.10 \text{ m}^{-1}$ and $b_0 = 0.0072 \text{ m}^{-1}$. The scattering phase function was the HG with $g = 0.85$, for which $\bar{b}_b = 0.036$. The total scattering coefficient corresponding to b_0 is $b_0/\bar{b}_b = 0.2 \text{ m}^{-1}$. Thus the range in values for the total attenuation coefficient $c(z) = a(z) + b(z)$ over the test cases in Table 2 is from 0.3 m^{-1} (a2bu at the minimum value) to 0.6 m^{-1} (a2b2 at the maximum value). These pseudodata were generated for an ocean illuminated with the Sun in a dark sky with $\theta_0 = 0$ and 60° and for an infinitely deep medium. The resulting $E_a(z)$ and $E_u(z)$ at 20 uniformly spaced depths from $z = 0$ to 4.75 m were then used as input to the algorithm described in Subsection 2.B and the profiles of $a(z)$ and $b_b(z)$ were retrieved. Note that the scales of variation of a and b_b are of the order of 1 m or larger. Thus the 0.25-m

Table 2. Gaussian Profile Parameters and Identification Code

z_a (m)	z_b (m)	a_1 (m^{-1})	b_1 (m^{-1})	Code
2	—	a_0	0	a2bu
—	2	0	b_0	aub2
2	2	a_0	b_0	a2b2
3	1	a_0	b_0	a3b1

separation between the points at which the pseudodata were provided was sufficient to completely resolve the vertical structure.

An example of the resulting retrieval is presented in Fig. 3(a), which provides the measured (filled circles) and the retrieved values of $R(z)$ for the aub2 case in Table 2 with $\theta_0 = 0$. The solid curve in Fig. 3(a) connects points at which $R(z)$ was reconstructed by use of the retrieved values of $a(z)$ and $b_b(z)$ when the correct phase function (HG, $g = 0.85$) was used in the retrievals. The dashed curve connects points of $R(z)$ reconstructed by use of the retrieved values of $a(z)$ and $b_b(z)$ when an incorrect phase function (HG, $g = 0.95$) was used in the retrieval algorithm. In both cases (retrieval with the correct and incorrect phase functions) the reconstructed $R(z)$ is within a fraction of a percent of the true values; however, the error is clearly larger when the incorrect phase function is used. Figures 3(b) and 3(c) provide the error in the retrieved values of $a(z)$ and $b_b(z)$, respectively. In these figures the solid and dashed curves have the same meaning as in Fig. 3(a). The errors in the retrieved $a(z)$ are seen to be slightly larger when the incorrect phase function is used in the retrieval, and there appears to be a systematic bias of ~ 1 – 1.5% for $z > 2$. The error in $a(z)$ follows the same pattern for the two retrievals. This is due to the fact that a significant portion of the error in $a(z)$ results from the computation of $K_v(z)$ in Eq. (1). This portion of the error is independent of the operation of the inversion algorithm, depending only on the accuracy of the numerical derivative that is used in the initial (and only) computation of $K_v(z)$. The error in this derivative sets the lower limit to the error in the algorithm. The reason our derivatives appear to have small random errors is that the pseudodata were generated with a Monte Carlo solution of the RTE, which inevitably contains statistical fluctuations. The increasing bias in $a(z)$ with increasing z when the incorrect phase function is used is due to $\bar{\mu}(z)$. It is clear that near the surface, $\bar{\mu}(z)$ is nearly independent of the phase function because the light field is dominated by the solar beam; however, as z increases, $\bar{\mu}(z)$ will begin to depend on $P(\Theta)$ through single and multiple scattering. This provides the increased error in $\bar{\mu}(z)$ with increasing z . Although the incorrect phase function is more strongly forward scattering, which would increase $\bar{\mu}(z)$ in the single-scattering approximation, the error in $\bar{\mu}(z)$ is increasingly negative with increasing z . This is caused by the increase in $b(z)$ required by the algorithm to provide an appropriate $b_b(z)$ when the incorrect phase

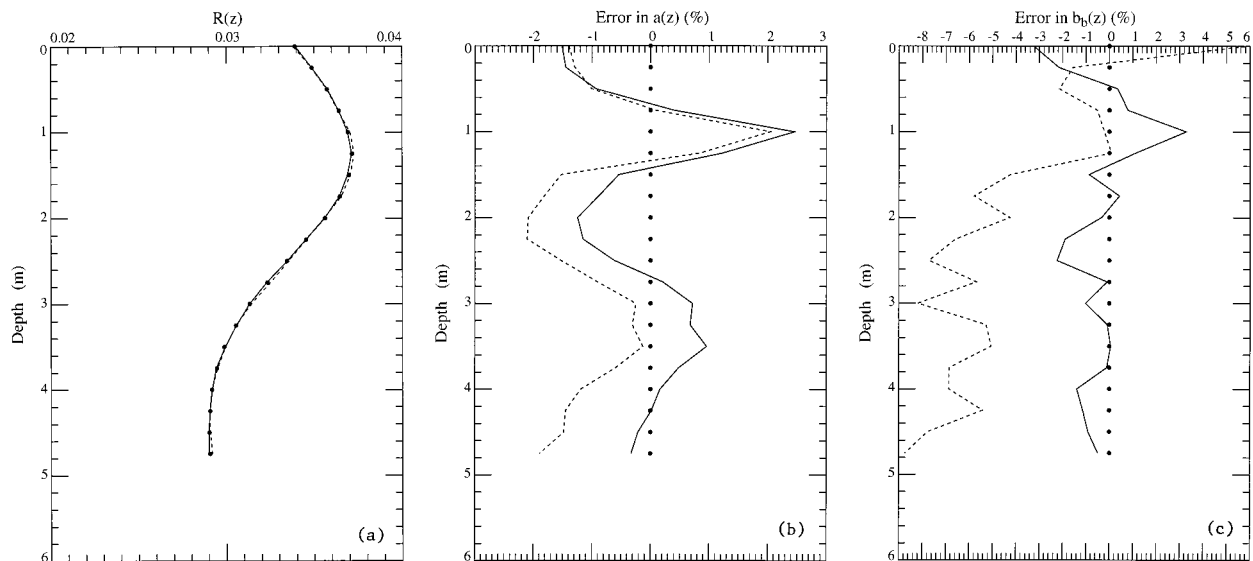


Fig. 3. Retrieval results for the case aub2 in Table 2. (a) $R(z)$ pseudodata (solid circles) and reconstructed values by use of $a(z)$ and $b_b(z)$ retrieved with the correct (solid curve) and an incorrect (dashed curve) phase function. (b) Percent error in $a(z)$ retrieved with the correct (solid curve) and an incorrect (dashed curve) phase function. (c) Percent error in $b_b(z)$ retrieved with the correct (solid curve) and an incorrect (dashed curve) phase function.

function (\widetilde{b}_b too small) is used. Larger values of $b(z)$ at fixed $a(z)$ result in more multiple scattering that tends to reduce $\bar{\mu}(z)$ when the Sun is at the zenith. Note, however, that the error in $\bar{\mu}(z)$ that is due to the incorrect phase function is $\leq 1.5\%$. The ability of the algorithm to provide an excellent estimate of $\bar{\mu}(z)$ is the reason for its robustness in the estimation of $a(z)$.

For $b_b(z)$ there is little bias when the correct phase function is used; however, with the incorrect phase function there is clearly a bias of $\sim 8\%$ for $z > 2$. It is important to note that when the incorrect phase function is used, $\widetilde{b}_b = 0.011$ compared with 0.036 for the correct phase function, i.e., the error in \widetilde{b}_b when the incorrect phase function is used is over a factor of 3. In contrast, the error in $b_b(z)$ induced by the incorrect phase function is $< 9\%$. A similar behavior was found for the homogeneous medium algorithm in Ref. 1.

Tables 3 and 4 provide summaries of the algorithm's performance for the cases listed in Table 2 when the correct and incorrect phase functions, respectively, are used in the retrievals. The tables list the depth-averaged absolute error [in the sense of Eq. (6)] in the quantities indicated. Clearly, the retrievals of $b_b(z)$ are better when the correct phase function is used in the retrievals; however, the phase function has little effect on the error in $a(z)$.

We also carried out simulations with stronger stratifications, e.g., with $a_1 = 4a_0$ and/or $b_1 = 4b_0$. The results are similar to those presented in Fig. 3 and Table 3; however, the errors were somewhat larger. The increase in error with increasing stratification appears to be due entirely to difficulty in computing the numerical derivatives required by the algorithm with a 0.25-m spacing between the samples.

C. L_u - E_d Algorithm Performance

For all cases described in Subsection 3.B, we retrieved the IOP's using the L_u - E_d algorithm as well. Tables 3 and 4 compare the performance of the L_u - E_d and E_u - E_d algorithms. Although there is some degradation in the accuracy of the retrieved $a(z)$, there is

Table 3. Depth Averages of the Absolute Error in $a(z)$ and $b_b(z)$ (percent) When the Correct Phase Function is Used in the Retrievals^a

Code	θ_0	$\langle \Delta a \rangle_{E_u}$	$\langle \Delta a \rangle_{L_u}$	$\langle \Delta b_b \rangle_{E_u}$	$\langle \Delta b_b \rangle_{L_u}$
a2bu	0°	0.67	0.70	1.38	2.08
a2bu	60°	0.85	1.02	1.80	1.61
aub2	0°	0.81	0.68	1.10	2.81
aub2	60°	0.88	1.20	1.31	3.16
a2b2	0°	1.52	1.72	1.32	2.32
a2b2	60°	1.38	1.92	1.56	1.79
a3b1	0°	1.05	1.11	1.52	1.93
a3b1	60°	1.28	1.21	1.32	1.70

^aThe subscripts E_u and L_u refer to retrievals made with the E_u - E_d and L_u - E_d algorithms, respectively.

Table 4. Depth Averages of the Absolute Error in $a(z)$ and $b_b(z)$ (percent) When an Incorrect Phase Function is Used in the Retrievals^a

Code	θ_0	$\langle \Delta a \rangle_{E_u}$	$\langle \Delta a \rangle_{L_u}$	$\langle \Delta b_b \rangle_{E_u}$	$\langle \Delta b_b \rangle_{L_u}$
a2bu	0°	0.90	1.35	3.34	7.24
a2bu	60°	1.23	1.51	5.76	5.56
aub2	0°	1.21	1.65	5.06	5.99
aub2	60°	1.24	2.30	8.07	8.42
a2b2	0°	1.23	1.45	3.96	4.88
a2b2	60°	1.28	1.59	6.66	5.87
a3b1	0°	1.65	1.39	4.62	4.48
a3b1	60°	1.88	2.18	7.02	7.32

^aThe subscripts E_u and L_u refer to retrievals made with the E_u - E_d and L_u - E_d algorithms, respectively.

little difference in the accuracy of the retrieved $b_b(z)$ for the cases that we examined.

4. Difficult-to-Handle Situations

In addition to the tests described in Section 3, we devised several tests to try to make the algorithm fail with large error. In this section we discuss cases in which the algorithm has difficulty deriving the IOP's: absorbing layers that are so thin that $K_v(z)$ cannot be estimated accurately, situations in which $dR(z)/dz$ is large and positive, and situations in which there is excessive noise in the input data.

A. Thin Absorbing Layers

When a thin (thickness defined as the spacing between irradiance samples) absorbing layer is encountered, the algorithm can produce large errors. As an example of this we generated pseudodata for E_u and E_d using $z_a = 2$, $a_1 = 4a_0$, $\sigma_a = 0.1$, and $b_1 = 0$. This provided a thin, strongly absorbing layer in an otherwise homogeneous medium. Approximately 68% of the additional absorption provided by this layer falls between $z = 1.90$ and 2.10 m, and 98.7% of the additional absorption is between $z = 1.75$ and 2.25 m. We found that, although large errors in a and b_b were encountered near $z = 2$, the algorithm performed well elsewhere.

To make recovery of the IOP's more difficult, we omitted the E_u-E_d pseudodata at a single depth, $z = 2$, the maximum in the $a(z)$ profile. In this case almost all the additional absorption near $z = 2$ is missed in the pseudodata. Figure 4 provides the results for both simulations: with the pseudodata present and with the pseudodata absent at $z = 2$ m. As expected, there are large errors in a and b_b near the absorbing layer. Interestingly, the error in b_b is not significantly altered by the absence of pseudodata at $z = 2$ m. In contrast, the absorbing layer is somewhat better delineated in a in the presence of pseudodata at $z = 2$ m.

The profiles of $E_d(z)$ and $R(z)$ derived by use of the recovered $a(z)$ and $b_b(z)$ are revealing. When the pseudodata at $z = 2$ m are omitted, the algorithm cannot identify the presence of the strongly absorbing layer, and the absence of this contribution to the absorption is reflected in a constant bias in the reconstructed $E_d(z)$ for $z > 2$ m. In this region ($z > 2$ m) there is no $a(z)$ that will remove the bias, e.g., a larger (smaller) $a(z)$ would increase (decrease) $K_v(z)$ thereby changing the slope as well as the magnitude of $\ln E_d$. Such a bias in $E_d(z)$ must result from missed absorption somewhere in the water column, and the shape of $E_d(z)$ clearly suggests it must be near $z = 2$ m. Similarly, although a and b_b are quite accurate for $z \leq 1.5$ m, the $R(z)$ profile cannot be reconstructed accurately in the absence of some knowledge of the presence of the absorbing layer.

These simulations demonstrate the importance of having samples with sufficiently close spacing so that thin absorption layers can be identified. They also demonstrate that the presence of such layers can be

ascertained by comparing the reconstructed and the true irradiance profiles.

B. Large Values of dR/dz

Equation (5) suggests that the algorithm will have difficulty if dR/dz is large and positive where R is small. Such a situation is possible with a strongly absorbing surface layer over a highly reflective layer below the surface. We examined a situation in which the pseudodata were generated by use of a two-layer model with $\omega_0 = 0.5$ from $z = 0$ to 2 m and $\omega_0 = 0.9$ from $z = 2$ m to ∞ . The phase function was a HG with $g = 0.85$. The retrieval algorithm assumed a HG phase function with $g = 0.95$. Huge errors were found in the retrieval, and these were traced to the fact that Eq. (5) produced negative values of $X(z)$ near the surface where R is small. When this happened, the default was to set $b_b(z)$ to a small positive number. The algorithm then proceeded to diverge. In fact, this is the only case we have ever run in which the algorithm clearly diverged. We ran this case again, but when Eq. (5) yielded a negative $X(z)$, the default was changed to replace the negative $X(z)$ by $X(z) = 3R(z)$, i.e., we set $dR/dz = 0$. This produced reasonable (not excellent) retrievals.

C. Excessive Noise in the Irradiances

The downward irradiance near the surface is generally strongly fluctuating in time because of the effects of surface waves. Thus the downward irradiances may have considerable random errors. These errors can cause a large error in derivatives, and this is especially significant in the case of $K_v(z)$. This fluctuation error is largest at the surface and decreases with depth.¹¹ We performed several tests in which random errors, decreasing in magnitude with depth, were applied to the pseudodata. The results suggest that the error in the computation of $K_v(z)$ is the most significant. Error in $K_v(z)$ leads to a similar error in $a(z)$ through Eq. (1). The error in $a(z)$ usually prevents the reconstructed $E_d(z)$ and $E_u(z)$ from fitting their pseudodata counterparts well. Biases usually appear that are similar in nature to those that would be induced by thin absorbing layers, e.g., Fig. 4. However, the reconstructed reflectance $R(z)$ usually follows the noisy $R(z)$ pseudodata reasonably well. Thus, given $a(z)$ (including its noise-induced error), the algorithm tries to determine a $b_b(z)$ that will reproduce the apparent $R(z)$. As the error in $R(z)$ is not correlated with the error in $E_d(z)$ because of the error in $E_u(z)$, the error in $a(z)$ and $b_b(z)$ show few similarities.

This problem is not really a flaw in the algorithm, but it is a problem that is common to any application of irradiance data in which the various irradiance attenuation coefficients are required. There has been much effort devoted toward analysis of irradiance data to produce accurate attenuation coefficients.¹² Improvements in such analysis must be incorporated into the present algorithm for its full utility to be realized.

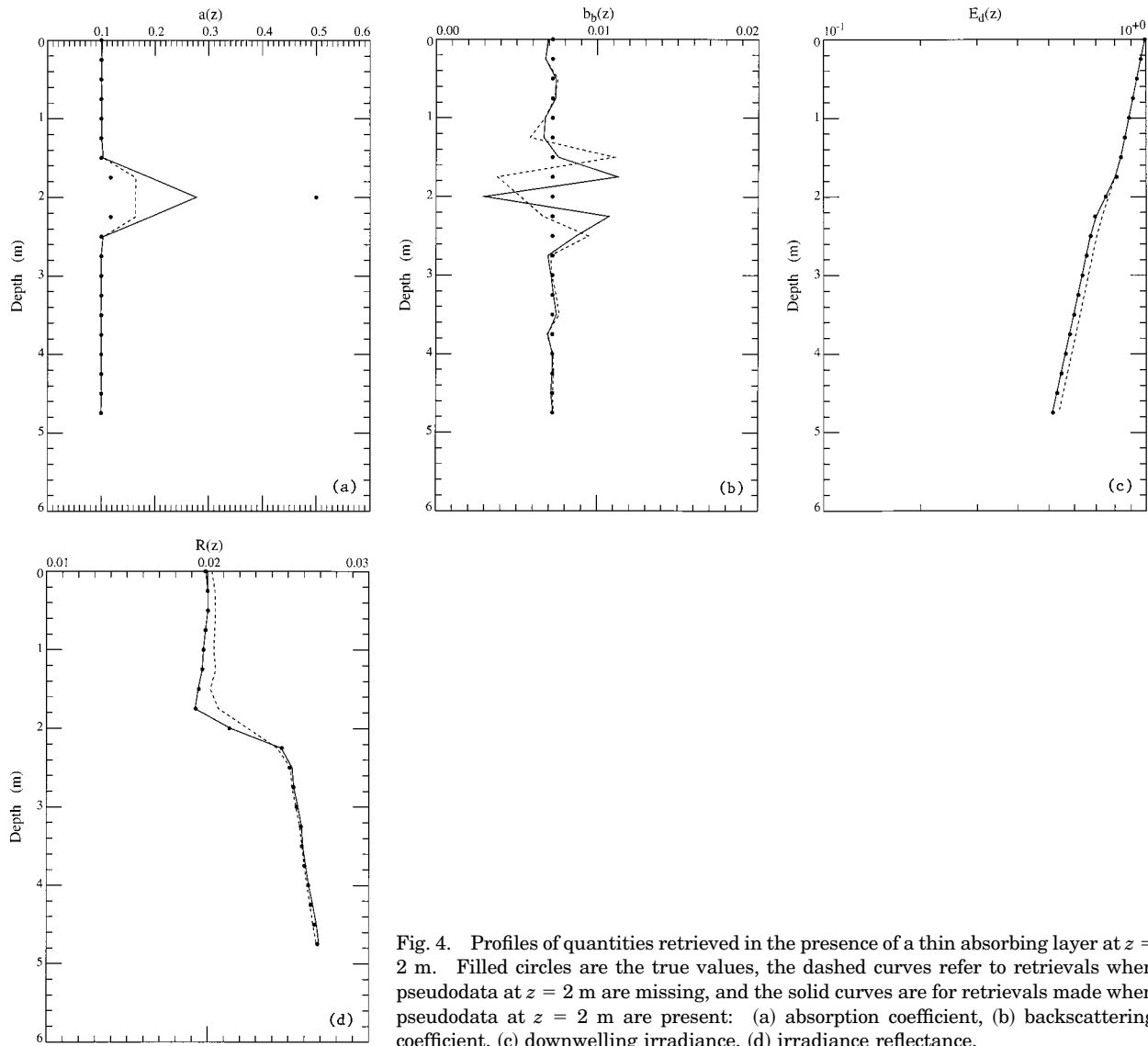


Fig. 4. Profiles of quantities retrieved in the presence of a thin absorbing layer at $z = 2$ m. Filled circles are the true values, the dashed curves refer to retrievals when pseudodata at $z = 2$ m are missing, and the solid curves are for retrievals made when pseudodata at $z = 2$ m are present: (a) absorption coefficient, (b) backscattering coefficient, (c) downwelling irradiance, (d) irradiance reflectance.

5. Depth Variations of $P(\Theta)$

In all the computations presented thus far, the phase function used in generating the pseudodata has been independent of depth. In reality, unless the medium is homogeneous, or there is no particle scattering, the phase function will vary somewhat with depth because the fraction of total scattering contributed by the water itself will vary as the particle concentration varies and because the phase function of the suspended particle population will generally vary with depth. To ascertain the effect of a depth-dependent phase function, we created pseudodata using the model provided in Mobley *et al.*⁹ (Problem 3) to relate the particulate absorption and scattering coefficients to the pigment concentration. The parameters of the Mobley *et al.* model were $h = 4 \text{ mg m}^{-2}$, $s = 0.5 \text{ m}$, $z_{\text{max}} = 2.25 \text{ m}$, and $C_0 = 0.005 \text{ mg m}^{-3}$. The wavelength was taken to be 500 nm at which the water absorption and backscattering coefficients are approximately 0.0257 and 0.00135 m^{-1} , respectively. With these parameters the pigment concentration

$C(z)$ ranged from ~ 0.005 to 3.2 mg m^{-3} , the absorption coefficient from ~ 0.027 to 0.106 m^{-1} , and the backscattering coefficient from ~ 0.0021 to 0.036 m^{-1} . The Rayleigh-scattering phase function was used for the scattering by the pure water component, and a depth-independent HG phase function with $g = 0.80$ was used for the particle-scattering component. Figure 5 shows the variation of the phase function from the smallest C value (dashed curve) to the largest C value (solid curve). At any depth, the phase function for the medium will fall between these two curves. The asymmetry parameter for the medium (combined Rayleigh and particle scattering) ranged from 0.648 to 0.797, and the total backscattering probability $0.0526 < \widetilde{b}_b(z) < 0.1365$, with the particle backscattering probability = 0.0507. Thus, over the depth profile, $\widetilde{b}_b(z)$ varied by a factor of ~ 3 and g varied by $\sim 25\%$. The pseudodata were created for the Sun at $\theta_0 = 0$ in a dark sky.

We retrieved $a(z)$ and $b_b(z)$ from the pseudodata

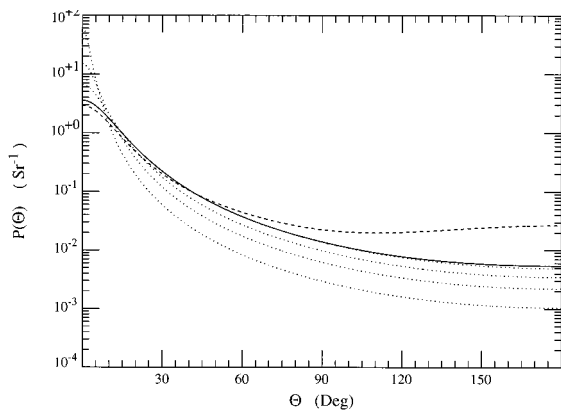


Fig. 5. Variation of the true phase function for the medium in Section 5 from the smallest (dashed curve) to the largest (solid curve) value of C . The dotted curves correspond to the HG phase functions for $g = 0.80, 0.85, 0.90,$ and 0.95 that were assumed in the retrievals. $P(\Theta)$ at large Θ is smaller for larger values of g .

described above assuming depth-independent HG phase functions with $g = 0.80, 0.85, 0.90,$ and 0.95 . These HG phase functions are provided as the dotted curves in Figure 5 (lower curves beyond $\Theta = 10^\circ$ correspond to larger values of g). Note that over the angular range $30^\circ < \Theta < 180^\circ$, all the retrieval phase functions fall below the range of the true phase function. Also, at low C values, the HG with $g = 0.90$ is almost an order of magnitude smaller than the true phase function for $\Theta \geq 150^\circ$. The resulting retrievals for $g = 0.80$ and 0.90 are presented in Fig. 6, in which the correct values are indicated by filled circles, the values retrieved by use of $g = 0.80$ by solid curves, and the values retrieved by use of $g = 0.90$ by dashed curves. Although the error is larger than that in Fig. 3, where the profile is much less extreme and the phase function is independent of depth, it is not excessive. The noisy appearance of the error in Fig. 6(c) suggests that the principal source in $a(z)$ is in the computation of $K_v(z)$, not in the assumption of a depth-independent phase function. Figure 6(d) shows understandable trends in the error in $b_b(z)$. In the region of high scattering the retrieval of $b_b(z)$ is excellent when $g = 0.80$ is assumed, as this value of g is nearly correct there; however, below the scattering maximum, where the contribution that is due to Rayleigh scattering becomes significant ($g \sim 0.65$), the assumed g is too large, leading to an even smaller $b_b(z)$. With an assumed $g = 0.90$, $b_b(z)$ is typically smaller than with $g = 0.80$. These trends in regard to $b_b(z)$ are similar to those in Fig. 3. It is remarkable that, when a phase function as radically different from the true phase function as the HG with $g = 0.90$ (Fig. 5) is assumed in the retrievals, errors of the order of only $\pm 20\%$ in the retrieved values of $b_b(z)$ are obtained (Fig. 6).

Table 5 provides a summary of the mean absolute error for a and b_b for the profiles used in this section. Note the almost complete independence of $\langle \Delta a \rangle$ on the value of g used in the retrievals. When $E_d(z)$ and $E_u(z)$ are reconstructed with the retrieved IOP's, er-

ror in $E_d(z)$ is always $< 0.5\%$, and the error in $E_u(z)$ is $< 1\%$, except for a single depth (when $g = 0.95$). Thus the quality of the fit of the reconstructed profiles to the input data does not provide information regarding the appropriateness of the assumed phase function.

We note that for the profile we use here the variation in the phase function with depth is significantly more extreme than what would be expected in natural waters. Therefore from this test we conclude that (1) use of a constant and incorrect phase function in the retrieval of $a(z)$ does not lead to excessive error in the absorption coefficient, and (2) the error in $b_b(z)$ appears to be directly related to the error in the assumed phase function, but again is not excessive.

6. Concluding Remarks

In this paper we have described an algorithm for estimation of profiles of the absorption and backscattering coefficients from profiles of the upwelling and downwelling irradiance or upwelling (nadir) radiance and downwelling irradiance. The key to extending the homogeneous water body algorithm¹ to a stratified water body is the presence of the $dR(z)/dz$ term in Eq. (5). Several tests of the algorithm in which we used simulated (pseudo) data were presented. They demonstrate that the algorithm can correctly determine the vertical structure of a stratified water body and usually provide $a(z)$ with an error $\leq 2\%$ and $b_b(z)$ with an error $\leq 10\%$ (Fig. 1–3, Tables 1–4), as long as the spacing between pseudodata samples is sufficiently small that the necessary derivatives [$K_v(z)$ and $dR(z)/dz$] can be computed accurately. The results are better the closer the phase function used in the retrievals is to the true phase function, although excellent retrievals of $a(z)$ can still be obtained with a very inaccurate phase function (Fig. 3, Table 4). This implies that the algorithm provides accurate estimates of the average cosine of the in-water radiance distribution $\bar{\mu}(z)$. The algorithm is able to provide realistic values of $b_b(z)$, even with an incorrect phase function, by adjusting $b(z)$ to provide a nearly correct $b_b(z)$; however, the resulting values of $b(z)$ are meaningless unless the correct phase function is used in the retrieval.^{1,13}

A test of the algorithm was devised to examine its performance in the presence of thin absorbing layers that cannot be completely resolved in $K_v(z)$, given the density of the pseudodata. As expected, the results showed very large error in $a(z)$ and $b_b(z)$ in the vicinity of the layer, but not elsewhere. Furthermore, the reconstructed $E_d(z)$ and $R(z)$ showed exceptionally large errors that could easily be ascribed to missed absorption [Figs. 4(c) and 4(d)].

Another test examined the quality of retrievals when the scattering phase function of the water body varies with depth. Using an unrealistically large variation in $P(\Theta)$ in the pseudodata, we showed that reasonably good retrievals were obtained (Table 5) with the largest error at depths where the phase function error was largest (Fig. 6).

The algorithm fails when Eq. (5) provides a nega-

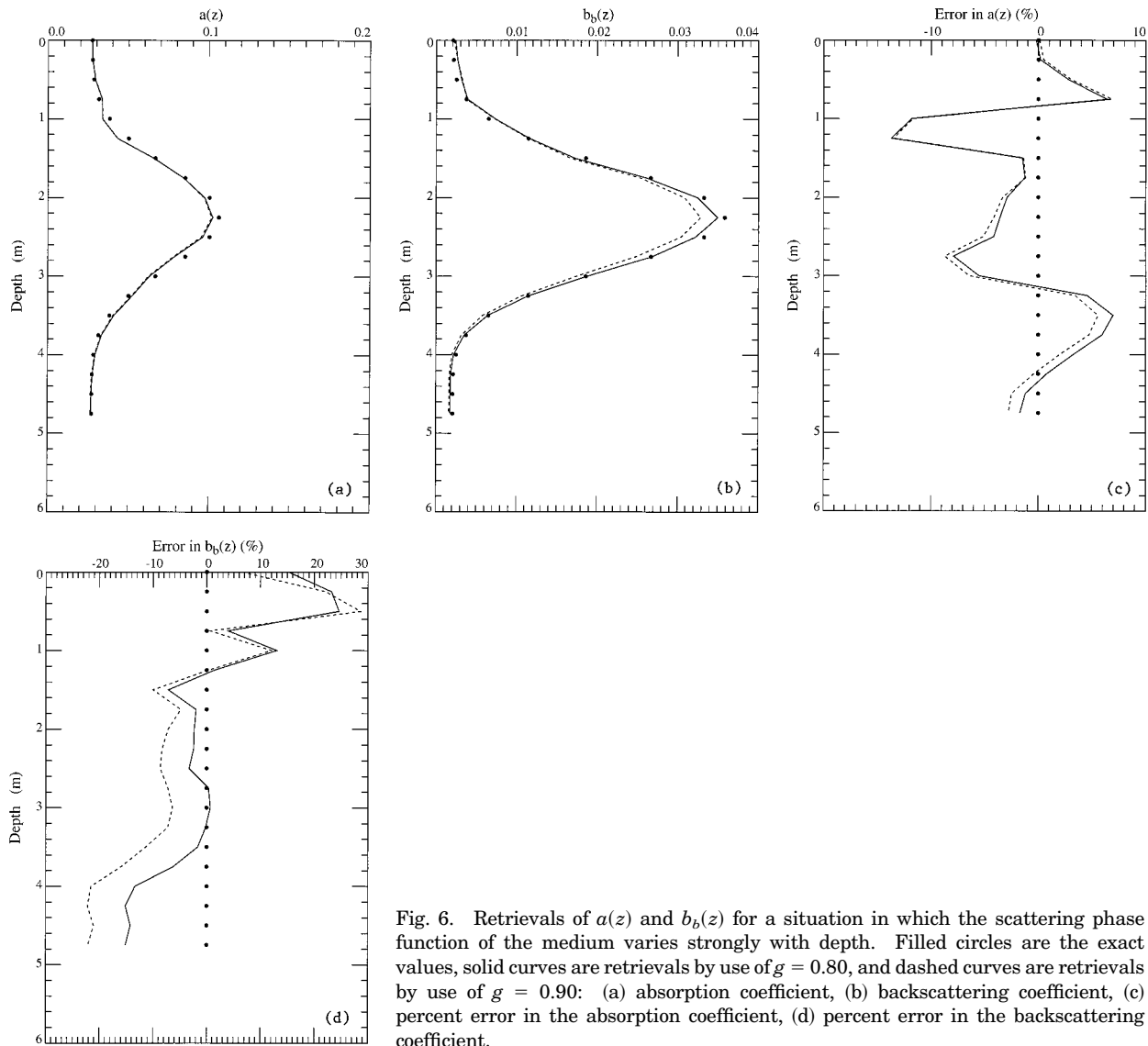


Fig. 6. Retrievals of $a(z)$ and $b_b(z)$ for a situation in which the scattering phase function of the medium varies strongly with depth. Filled circles are the exact values, solid curves are retrievals by use of $g = 0.80$, and dashed curves are retrievals by use of $g = 0.90$: (a) absorption coefficient, (b) backscattering coefficient, (c) percent error in the absorption coefficient, (d) percent error in the backscattering coefficient.

tive value of $X(z)$ at some depth; although by defaulting to $X(z) = 3R(z)$ where this happens, reasonable retrievals were obtained. It is also sensitive to noise in the irradiances mainly through error in the computation of $K_v(z)$; however, as most applications of in-water irradiance measurements involve computation of such attenuation coefficients (see, e.g., Ref. 2), this is not considered to be a blemish.

Table 5. Depth-Averaged Absolute Error [Eq. (6)] in Percent Obtained for $a(z)$ and $b_b(z)$ ^a

g	$\langle \Delta a \rangle$	$\langle \Delta b_b \rangle$
0.80	4.29	8.86
0.85	4.39	10.55
0.90	4.35	14.43
0.95	4.58	14.32

^aCalculated as a function of the value of g used in the retrieval for the depth-dependent $P(\theta)$ test in Section 5.

Although we have provided only tests of the algorithm for the Sun in a dark sky, i.e., in the absence of the atmosphere, our radiative transfer code, that serves as a subroutine in the algorithm, contains a 50-layer atmosphere that can include aerosol as well as Rayleigh scattering. In any cloud-free application of the algorithm, the atmosphere (at least the molecular-scattering component, and an aerosol component if possible) should be included. However, as we are using irradiances, precise definition of the aerosol part is not necessary. In case of a completely overcast sky, the atmosphere should be replaced by either a uniform or a cardioidal² incident radiance distribution on the sea surface. A sky with patchy clouds presents a difficult problem. The best solution would be to measure the radiance distribution falling on the sea surface¹⁴ and use it in the radiative transfer computation. A less accurate approximation would be to measure the individual contributions to the incident irradiance from the Sun and sky and

then model the sky contribution as a uniform (or some other) radiance distribution.¹⁵

In its present form the algorithm should be applied only to data acquired down to depths above which $dR(z)/dz = 0$, as was assumed in Eq. (5). As with all radiative transfer applications that ignore the possibility of inelastic scattering, this algorithm can be used only in spectral regions and at depths where inelastic scattering can be considered negligible. When this is not the case, it can be applied only when the inelastic component is estimated, e.g., by examination of solar Fraunhofer lines.¹⁶

Finally, we have tried here to provide the reader with samples of retrievals and with a short assessment of the accuracy of, and difficulties with, the algorithm. As such, there is no way our analysis can be exhaustive. Anyone using this algorithm should carry out a sensitivity study that is specific to the characteristics of their measurements and the conditions under which they were obtained.

The authors are grateful to the U.S. Office of Naval Research for support under grant N00014-97-I-0069.

References

1. H. R. Gordon and G. C. Boynton, "Radiance-irradiance inversion algorithm for estimating the absorption and backscattering coefficients of natural waters: homogeneous waters," *Appl. Opt.* **36**, 2636–2641 (1997).
2. C. D. Mobley, *Light and Water; Radiative Transfer in Natural Waters* (Academic, New York, 1994).
3. H. R. Gordon, O. B. Brown, and M. M. Jacobs, "Computed relationships between the inherent and apparent optical properties of a flat homogeneous ocean," *Appl. Opt.* **14**, 417–427 (1975).
4. A. Morel and L. Prieur, "Analysis of variations in ocean color," *Limnol. Oceanogr.* **22**, 709–722 (1977).
5. H. R. Gordon and W. R. McCluney, "Estimation of the depth of sunlight penetration in the sea for remote sensing," *Appl. Opt.* **14**, 413–416 (1975).
6. H. R. Gordon, "Remote sensing of optical properties in continuously stratified waters," *Appl. Opt.* **17**, 1893–1897 (1978).
7. H. R. Gordon and D. K. Clark, "Remote sensing optical properties of a stratified ocean: an improved interpretation," *Appl. Opt.* **19**, 3428–3430 (1980).
8. W. H. Press, B. P. Flannery, S. A. Teukolsky, and W. T. Vetterling, *Numerical Recipes in FORTRAN* (Cambridge University, Cambridge, England, 1992).
9. C. D. Mobley, B. Gentili, H. R. Gordon, Z. Jin, G. W. Kattawar, A. Morel, P. Reinersman, K. Stamnes, and R. H. Stavn, "Comparison of numerical models for computing underwater light fields," *Appl. Opt.* **32**, 7484–7504 (1993).
10. G. W. Kattawar, "A three-parameter analytic phase function for multiple scattering calculations," *J. Quant. Spectrosc. Radiat. Transfer* **15**, 839–849 (1975).
11. J. Dera and H. R. Gordon, "Light field fluctuations in the photic zone," *Limnol. Oceanogr.* **13**, 697–699 (1968).
12. D. A. Siegal, M. C. O'Brien, J. C. Sorensen, D. A. Konnoff, E. A. Brody, J. L. Mueller, C. O. Davis, W. G. Rhea, and S. B. Hooker, "Results of the SeaWiFS Data Analysis Round-Robin (DARR-94)," Vol. 26 of SeaWiFS Technical Report Series NASA Tech. Memor. 104566 (July 1994).
13. H. R. Gordon, "The sensitivity of radiative transfer to small-angle scattering in the ocean: a quantitative assessment," *Appl. Opt.* **32**, 7505–7511 (1993).
14. G. Zibordi and K. J. Voss, "Geometrical and spectral distribution of sky radiance: comparison between simulations and field measurements," *Remote Sensing Environ.* **27**, 343–358 (1989).
15. H. R. Gordon, "Can the Lambert-Beer law be applied to the diffuse attenuation coefficient of ocean water?," *Limnol. Oceanogr.* **34**, 1389–1409 (1989).
16. Y. Ge, K. J. Voss, and H. R. Gordon, "In situ measurements of inelastic scattering in Monterey Bay using solar Fraunhofer lines," *J. Geophys. Res.* **100**, 13,227–13,236 (1995).